The Making of the DRAKKAR FORCING SET DFS5

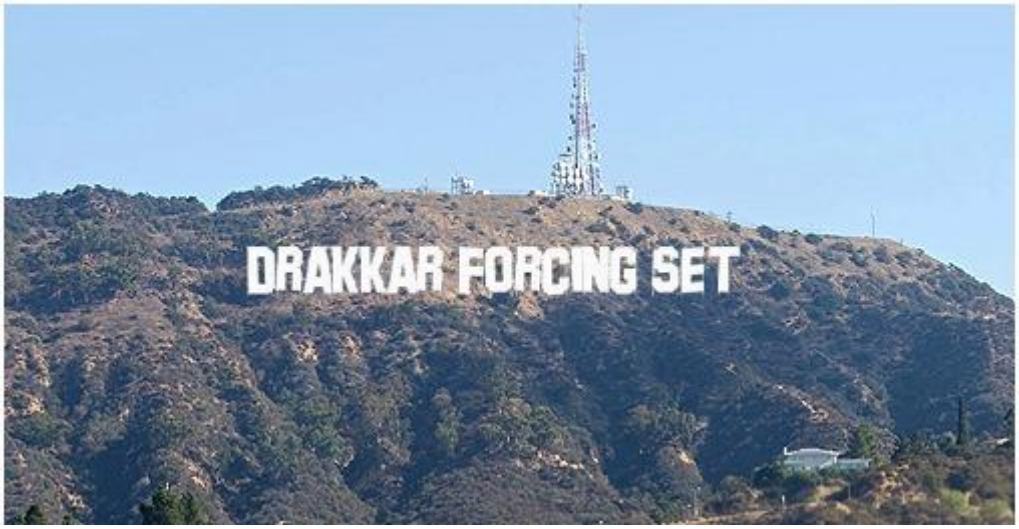

Raphael Dussin*, Bernard Barnier

MultiscalE Ocean Modelling (MEOM) Team
Laboratoire de Glaciologie et Géophysique de l'Environnement
CNRS, Université de Grenoble, OSUG, Grenoble, France
**Now at Institute of Marine and Coastal Sciences, Rutgers University, New Brunswick,USA*

Laurent Brodeau
Department of Meteorology, Stockholm University, Stockholm, Sweden

Contact Email
bernard.barnier@legi.grenoble-inp.fr

DRAKKAR/MyOcean Report 05-10-14

PROVISORY VERSION

May 2014

Table of content

1 Introduction

1.1 Context

Simulating the evolution of the global ocean over the last few decades using Ocean General Circulation models (OGCMs) has been made possible since globally gridded inter-annual weather reanalysis products have become available. Atmospheric fields from these reanalyzes are used to estimate fluxes to be applied as surface boundary conditions for OGCMs. In this context, DRAKKAR[1] is using atmospheric reanalyses carried out at the European Centre for Medium Range Weather Forecast (ECMWF) to develop data sets (referred to as the Drakkar Forcing Sets, DFS) intended to drive ocean hindcasts simulations of the last five decades (1958 to present). DRAKKAR produced several forcing data sets based on the ERA40 reanalysis and ECMWF real-time analyses (see Brodeau et al., 2010). Widely used, these data sets (DFS3 and DFS4) provide the surface meteorological variables required as input by the NEMO-based hierarchy of model configurations to calculate the air-sea fluxes that drive hindcasts simulations. The present report describes the making of latest forcing set, the DFS5, mainly based on the recent reanalysis ERA-interim (ERAi hereafter).

This report is organised as follows. A brief description of the previous DFS3 and DFS4, and a summary of the characteristics of the DFS5 forcing data set are presented in Section 1. Section 2 is a very short assessment of the original ERAi as a forcing of an ocean model. Section 3 describes in details the corrections applied to the original ERAi to provide the intermediate forcing data set DFS5.1 for the period 1979-2010. Section 4 exposes how DFS5.1 is extended backward in time from 1979 until 1958 using ERAi and ERA40, to finally achieve the final DFS5 forcing set for the period 1958 to 2012 (2013 being processed). Section 5 presents an atlas that illustrates the effect of the corrections by comparingDFS5 to the original ERAi.

1.2 Brief description of the previous DFS

This section briefly recalls the main characteristics of the previous Drakkar Forcing Sets that have been used to drive ocean hindcasts of the period 1958 to present (see also Table 1). All DFS forcings comprise the following surface variables required by the NEMO bulk formula to calculate heat, freshwater and momentum fluxes across the air-sea interface that are the surface boundary condition to the model primitive equations.

- zonal and meridional components of the 10-m wind : *u10*, *v10*
- 2-m air humidity : *q2*
- 2-m air temperature : *t2*
- downward shortwave radiation at the sea surface : *radsw*
- downward longwave radiation at the sea surface : *radlw*
- precipitation total and solid : *P*, *snow*

[1] *DRAKKAR (http://www.drakkar-ocean.eu/) is a scientific and technical coordination between French research teams (LEGI-Grenoble, LPO-Brest, LOCEAN-Paris), MERCATOR-ocean, NOC Southampton, IFM-Geomar Kiel, and other teams in Europe and Canada. We propose to design, carry out, assess, and distribute high-resolution global ocean/sea-ice numerical simulations based on the NEMO platform (www.nemo-ocean.eu) performed over long periods (five decades or more), and to improve and maintain a hierarchy of state-of-the-art ocean/sea-ice model configurations for operational and research applications.*

1.2.1 DFS3 (period 1958-2007)

The DFS3 forcing function covers the period 1958-2007. The reference for this forcing data set is the DFS3 data set described in the paper by Brodeau et al. (2010). The ORCA025 reference experiment driven with DFS3 is ORCA025.G70. DFS3 combines elements from two sources. The CORE_v1 forcing data set (Large and Yeager, 2004), from which precipitation (rain *P*, and *snow*), downward shortwave (*radsw*) and longwave (*radlw*) radiations are extracted. The ERA40 reanalysis (for the period 1958-2001) and ECMWF operational analysis (2002-2007) which provides the 10-m wind (*u10*, *v10*), the 2-m air humidity (*q2*) and 2-m air temperature (*t2*) to compute turbulent air/sea and air/sea-ice fluxes during model integration. The frequency of DFS3 is monthly for precipitation and daily for radiation (both on the NCEP 1.875° grid), and 6-hourly for turbulent variables (on the 1.125° ERA40 grid). Note that climatological values are used for downward radiation and precipitation before 1979 as in CORE_v1 (see Table 1). The global heat and freshwater budgets (+12.8 Wm^{-2} and +56 mm/y, respectively) are not closed in DFS3.

1.2.2 DFS4.1 (1958-2007)

The DFS4.1 forcing function is a significant evolution of DFS3. Corrections have been applied to ECMWF variables (used in the calculation of the turbulent fluxes to remove unrealistic time discontinuities induced by changes in the nature of assimilated observations, by continuing ERA40 with ECMWF operational analyses, and to correct for obvious global and regional biases in ERA40 fields identified by comparison to high quality observations (see Brodeau et al., 2010). Winds have been rescaled such that the climatological mean matches that of the QuickScat winds. Air temperature and humidity have been corrected (i.e. cooled and dried) in the Arctic according to the POLES climatology (Rigor et al., 2000). Radiation fields are from ISCCP-FD (Zhang et al., 2004) with the reduction of 5% as proposed in CORE_v1. Precipitation is from the GXGXS data set (Large and Yeager, 2004). Both radiation and Precipitation have been submitted to small adjustments (in zonal mean) that yield a near-zero global imbalance of heat and freshwater when fluxes are estimated with the observed SST of Hurrell et al. (2008). The frequency and grid of DFS4.1 are as in DFS3 (see Table 1).

1.2.3 DSF4.2 (1958-2007)

DFS4.2 is a small evolution of DFS4.1. The scaling coefficient applied to the 10m wind is slightly reduced by limiting the amplitude of the correction to a maximum of 15% (considering that QuickScat may overestimate the surface wind speed). A very small correction of t2m and q2m (corresponding to an offset of 0.25°C) is added in the latitude band 55°N-65°N for a better continuity POLES in the Arctic.

1.2.4 DFS4.3 (1958-2007, extended to 2010)

For the period 1958-2007, DFS4.3 is exactly the DFS4 described in the Brodeau et al (2010) paper. It basically uses the corrections made and tested in DFS4.1 and DFS4.2, and adds new ones in order to close the heat and freshwater budgets.

Corrections applied to the 10 m wind and to the 2 m air temperature and humidity to remove the unrealistic time discontinuities induced by the changes in the nature of assimilated observations, or the change to ECMWF operational forecasts after 2001, are retained as defined in DFS4.1 and DFS4.2.

Corrections of applied to 2 m air temperature and humidity (i.e. cooled and dried) in the Arctic according to the POLES climatology with the small correction (equivalent to a

0.25°C offset) added in the latitude band 55°N-65°N for a smoother connection with POLES, are retained as defined in DFS4.1 and DFS4.2.

Rescaling of the 10 m wind speed according to QuickScat in the band 60°S-60°N is retained as defined in DFS4.1 and DFS4.2. *In DFS4.3 the maximum amplitude of the rescaling is bounded to a maximum of 15%.*

Radiation fields from ISCCP-FD (Zhang et al., 2004) are reduced by 7 in the inter-tropics, in a way similar that what was proposed by Large and Yeager (2004) for CORE_v1 (with a lesser reduction of 5%).

Precipitation from the GXGXS data set (Large and Yeager, 2004) are increased by 10% between 20°S-20°N to reach the values proposed by Trocolli and Kallberg (2004), and by 5% elsewhere.

Those adjustments yield a near-zero global imbalance of heat budget (+0.3 Wm^{-2}) and freshwater budget (-0.2 mm/y) when fluxes are estimated with the observed SST of Hurrell et al. (2008). The extension for 2008 to 2010 uses ERAi for the surface variables used in the calculation of the turbulent fluxes (u10, v10, t2, q2), and applies the persistence of year 2007 for the radiation fluxes and precipitation.

1.2.5 DFS4.4 (1958-2012)

DFS4.4 is the last forcing set of the DFS4 series (see Table 1 for a summary of characterisitcs). It is identical to DFS4.3 until 2001. The major evolution concerns the period from 2002 to 2012. For that period DFS4.4 uses ERAi for *every forcing variable* (i.e. the surface atmospheric variables used in the calculation of the turbulent fluxes, but also the downward longwave and shortwave radiation and rain/snow precipitation) in the following way. First the 3-hourly ERAi is interpolated in space onto DFS4.3 grids (the ERA40 grid for t2/q2/u10/v10, the CORE grid for radsw/radlw/P/Snow) and degraded to the DFS4.3 frequencies (to 6 hourly snatshots for the turbulent state variables, to daily mean for the downward radiation fluxes, and to monthly mean for the precipitation/snow). Then, "*high frequency residues*" are calculated as the difference between instantaneous original ERAi fields and the ERAi daily (monthly for precipitation) mean climatology (calculated over the period 1979-2001 common to ERA40 and ERAi). These "*residues*" are 6 hourly for the turbulent variables, daily for radiation and monthly for precipitation. Then these "*residues*" are added to the daily (monthly for precipitation) climatology of DFS4.3 (also calculated over the common period) to provide the final DFS4.4 fields, the resolution (time and grid) of which is identical to that of DFS4.3 (see Table 1).

1.2.6 DFS4.4_clim

A seasonal climatological forcing has been calculated from DFS4.4, which required a specific processing to account for the non linearity of the bulk formula. First and daily mean climatology is calculated for variables t2, q2 radsw, radlw by a simple time averaging of the 6-hourly or daily values over the whole 1958-2012 period. We then apply a 2-passes hanning filter, and we obtain 360 climatological days.

For the wind, using the daily climatology of u10 and v10 in the bulk formula will result in an underestimation of the momentum and heat input of at least 20 to 30%. Bulk formulas are such that it is the wind speed $w10 = (u10^2+v10^2)^{1/2}$ and the components of the pseudo stress *w10.u10, w10.v10* that are used. We therefore we calculated the daily climatology of these terms, with a 2-passes hanning. DFS4.4clim has consequently one additional variable, *w10*, and the zonal and meridional components of the wind are replaced by the zonal and meridional

components of the pseudo-stress. Note that *w10* is used in the calculation of the exchange coefficients. The non-linear effect induced in the high frequency variations of the wind on the fluxes is therefore better represnted. DFS4.4_clim has been used for long climatological runs (the ORCA12.L46.GJM02 run for 85 years). Differences in net heat flux between the two data sets over the whole period generally range between ±5 W.m^{-2}, with however greater differences (up to 20 W.m^{-2}) seen in western boundary (Figure below).

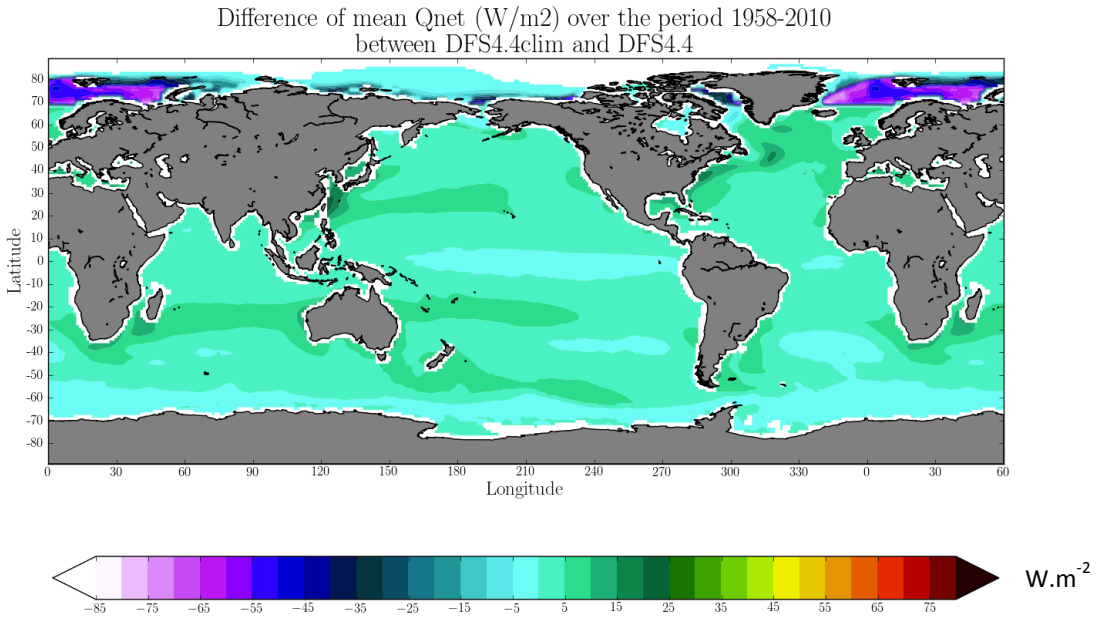

Figure: Net heat flux difference between DFS4.4-clim and DFS4.4 for the period 1958-2010.

Table 1: Major characteristics of the DFS3 and DFS4 data sets.

<table>
<tr><th rowspan="2">Variable name</th><th rowspan="2">Description</th><th rowspan="2">Units</th><th colspan="3">DFS3 Origin, time and grid resolution</th><th colspan="3">DFS4.3 Origin, time and grid resolution</th><th colspan="3">DFS4.4 Origin, time and grid resolution</th></tr>
<tr><th>1958-1978</th><th>1979-2001</th><th>2002-2007</th><th>1958-1978</th><th>1978-2001</th><th>2002-2010</th><th>1958-1978</th><th>1979-2001</th><th>2002-2012</th></tr>
<tr><td>u10</td><td>Zonal wind speed at 10 m height</td><td>m.s^{-1}</td><td colspan="2" rowspan="4">ERA40
6h
1.125°</td><td rowspan="4">ECMWF operational analyses
6h
1.125°</td><td colspan="2" rowspan="4">ERA40*
6h
1.125°</td><td rowspan="4">ECMWF operational analyses until 2007 and ERAi after
6h
1.125°</td><td colspan="2" rowspan="4">ERA40*
6h
1.125°</td><td rowspan="4">ERAi**
6h
1.125°</td></tr>
<tr><td>v10</td><td>Meridional wind speed at 10 m height</td><td>m.s^{-1}</td></tr>
<tr><td>t2</td><td>Air temperature at 2 m height</td><td>°C</td></tr>
<tr><td>q2</td><td>Air specific humidity at 2 m height</td><td>kg/kg</td></tr>
<tr><td>radsw</td><td>Downward shortwave radiation</td><td>W.m^{-2}</td><td>CORE
daily
climatology
1.875°</td><td colspan="2">CORE
daily
1.875°</td><td>ISCCP*
daily
climatology
1.875°</td><td colspan="2">ISCCP*
daily
1.875°</td><td>ISCCP*
daily
climatology
1.875°</td><td>ISCCP*
daily
1.875°</td><td rowspan="3">ERAi**
daily
1.125°</td></tr>
<tr><td>radlw</td><td>Downward longwave radiation</td><td>W.m^{-2}</td></tr>
<tr><td>P</td><td>Total precipitation</td><td>mm/day</td><td rowspan="2">CORE
monthly
climatology
1.875°</td><td colspan="2" rowspan="2">CORE
monthly
1.875°</td><td>GXGXS*
monthly
climatology
1.875°</td><td colspan="2" rowspan="2">GXGXS*
monthly
1.875°</td><td>GXGXS*
monthly
climatology
1.875°</td><td>GXGXS*
monthly
1.875°</td></tr>
<tr><td>snow</td><td>Snow fall</td><td>mm/day</td></tr>
<tr><td colspan="12">* : With corrections as described in Brodeau et al. (2010) to reduce time discontinuities when matching different data sets and to reach a nearly closed global balance.
** : ERAi 6 hourly residues (calculated as the difference between instantaneous original ERAi fields and the ERAi daily mean climatology of the period 1979-2001) are added to the climatological daily mean (period 1979-2001) of DFS4.4.</td></tr>
</table>

1.3 Short description of DFS5.2 (1958-present)

The DFS5.2 data set has been built to take advantage of ERA-interim, the most recent atmospheric reanalysis produced at ECMWF (Dee et al., 2011). ERAi provides the surface atmospheric variables required to drive global ocean hindcasts simulations for the period 1979-2012 and beyond), every 3 hours on a regular grid of resolution ~0.7°. Compared to previous reanalyses, it has the great advantage of an increased spatial resolution and denser time sampling that resolves the diurnal cycle. However, ERAi is limited to the period 1979-present, and has to be combined to another data set, i.e. ERA40 which does include the period 1958-1978. DFS5.2 has been constructed following a 3 step methodology.

1.3.1 Summary of the methodology

The first step is an assessment of ERAi forcing variables, described in Section 2. ERAi surface variables have been (i) compared to other products and (ii) used to drive global ocean hindcasts over the period 1979-2010 with the ORCA025[2] configurations. This preliminary work guided the needs for corrections.

The second step defined and applied a set of corrections to ERAi forcing variables for the period 1979-2010. It is described in Section 3. Hindcasts simulations long of 32 years are carried out with the 2° resolution ORCA2[3] model configuration to assess the sensitivity of the model to the proposed corrections. This yielded the DFS5.1 forcing, a short summary of which is described in the next Section 1.3.2. Finally, DFS5.1 is extended backward in time until 1958 using the ERA40 reanalysis. The methodology uses the 23 year period common to both data sets (1979-2001) to match ERA40 fluxes to those of DFS5.1 in a continuous way. This process, which is described in Section 5, yields the DFS5.1*e* (*e* for extended) which covers the period 1958-2010. Assessment of DFS5.1*e* has been carried out with ocean hindcasts at 2° and 1/4° resolution.

The third step built the DFS5.2 data set (1958-2012) which will be the reference forcing data set for sometimes, and the previous DFS will not be maintained. For the period 1979-2012, it is similar to DFS5.1 except for the following corrections that have been applied: Cooling/Drying of t2/q2 in the Antarctic, amplitude of the wind scaling to Quickscat set to 1 (instead of 0.8), modification of the radiation fluxes to re-equilibrate the global heat balance, and a slightly different way to apply the correction of Storto to the precipitation. The methodology to extend DFS5.2 over the period 1958-1978 is also slightly different from that used for DFS5.1. This is described in section 3 (*work in progress*).

The effect of the corrections is further investigated by comparing DFS5.2 and ERAi on the period 1979-2010 (Section 4 *work in progress*).

DFS5.2 has recently been extended until 2012, and will soon be extended to 2013.

1.3.2 DFS5.1 forcing (1958-2010)

DFS5.1 is based on the ERAi reanalysis. DFS5.1 provides downward shortwave and longwave radiation, precipitation, 10-m wind, 2-m air humidity and 2-m air temperature to compute turbulent air/sea and air/sea-ice fluxes and net radiation fluxes during model integration.
Period 1979-2010. The frequency of DFS5.1 over this period is 3 hourly for wind, air temperature and humidity, and daily for radiation and precipitation (an analytical diurnal

[2] *ORCA025 is the eddy-permitting, 1/4° resolution, global configuration of the Drakkar hierarchy of models (Barnier et al., 2006).*
[3] *ORCA2 is the coarse, 2° resolution, global configuration of the Drakkar hierarchy of models (Drakkar, 2007).*

forcing can be used for the solar flux in NEMO if desired). The spatial resolution is nearly 0.7°. Corrections have been applied to ERAi variables following an approach comparable to that of Brodeau et al. (2010) to reduce obvious global and regional biases (by comparison to high quality observations). Radiations have been corrected by comparison to the GEWEX radiation fluxes (Pinker and Laszlo, 1995). The wind speed has been corrected (i.e. increased) in the inter-tropical band by comparison to the Qscat wind climatology. Air temperature and humidity have been corrected (i.e. cooled and dried) in the Arctic according to the POLES climatology (Rigor et al., 2000), and in the southern ocean near the Antarctic continent according to a downscaling of ERA40 with a regional model (Mathiot et al., 2010). The greatest correction was applied to the precipitation fields to remove unrealistic time discontinuities (induced by changes in the nature of assimilated observations) and correct for excessive precipitation in the inter-tropical band, following the approach proposed by Storto et al. (2012). Corrections are fully described in Section 3.

Period (1958-1978). The DFS5.1 defined above over the period 1979-2010 is extended backward in time for the period 1958-1978 (Table 2). For the 1958-1978 period, radiation (shortwave and longwave downward radiation) and freshwater fluxes (total precipitation and snow) are the daily climatology of DFS5.1 (being calculated over the period 1979-2010). This was also the strategy for DFS4 and for CORE. The backward extension of the surface atmospheric variables required for the calculation of turbulent fluxes (t2, q2, u10 and v10) makes use of the ERA40 reanalysis. The synoptic scales (6-hourly) of ERA40 of the period 1958-1978 are retained but the daily mean climatology of ERA40 is replaced by that of DFS5.1 calculated on the period common to both data sets (1979-2001). To provide a homogeneous record, all fields are provided on a 0.7° grid, every 3h for the turbulent variables and daily for radiation and precipitation.

Table 2: Major characteristics of the DFS5.1 forcing data set.

<table>
<tr><th rowspan="2">Variable name</th><th rowspan="2">Description</th><th rowspan="2">Units</th><th colspan="2">DFS5.1 Origin, time and grid resolution</th></tr>
<tr><th>1958-1978</th><th>1979-200710</th></tr>
<tr><td>u10</td><td>Zonal wind speed at 10 m height</td><td>$m.s^{-1}$</td><td rowspan="4">ERAi* daily climatology (1979-2001) combined with ERA40** 3-hourly synoptic scales (1958-1978) 0.7° resolution</td><td rowspan="4">ERAi* 3-hourly 0.7° resolution</td></tr>
<tr><td>v10</td><td>Meridional wind speed at 10 m height</td><td>$m.s^{-1}$</td></tr>
<tr><td>t2</td><td>Air temperature at 2 m height</td><td>°C</td></tr>
<tr><td>q2</td><td>Air specific humidity at 2 m height</td><td>kg/kg</td></tr>
<tr><td>radsw</td><td>Downward shortwave radiation</td><td>$W.m^{-2}$</td><td rowspan="2">ERAi* daily climatology (1979-2010) 0.7° resolution</td><td rowspan="2">ERA-interim daily 0.7° resolution</td></tr>
<tr><td>radlw</td><td>Downward longwave radiation</td><td>$W.m^{-2}$</td></tr>
<tr><td>P</td><td>Total precipitation</td><td>mm/day</td><td rowspan="2">ERAi* daily climatology (1979-2010) 0.7° resolution</td><td rowspan="2">ERA-interim daily 0.7° resolution</td></tr>
<tr><td>snow</td><td>Snow fall</td><td>mm/day</td></tr>
<tr><td colspan="5">* ERAi* = ERA-interim variables after implementation of the corrections described in Section 3.
** ERA40 resolution is 6-hourly and 1.125°. To provide a homogeneous record, ERA40 have been interpolated at the resolution of ERAi (3-hourly and 0.7°).</td></tr>
</table>

DFS5.1 global heat budget is -2.24 Wm^{-2}. The fresh water imbalance (E-P) is 0.94 mm/day. Those budgets have benn calculated with the bulk formulas provided by Large and Yeager and the SST of Hurell et al. (2007).

1.3.3 DFS5.2 forcing (1958-2012).

DFS5.2 data set (1958-2012) which will be the reference forcing data set for some times, and the previous DFS will not be maintained.

Period 1979-2012. DFS5.2 is similar to DFS5.1 except for additional corrections that have been applied:

- Cooling/Drying of t2/q2 in the Antarctic (the cooling start at 60°S and linearly increases to reach 2°C at 75°S).
- Amplitude of the wind scaling to Quickscat set to 1 (instead of 0.8),
- Correction of the radiation fluxes to re-equilibrate the global heat balance,
- different way to apply the detrending and the correction of Storto to the precipitation. A multiplicative factor of 1.13 (13% increase) must be applied, preferably between the southernmost latitudes up to 50°N to bring the freshwater balance close to equilibrium (work in progress). Note that the use of the COARE bulk formula instead of the NCAR formula used in CORE would make that correction unnecessary (COARE produces smaller evaporation).

Period 1958-1978. The extension backward in time is also slightly different from that used for DFS5.1. Radiation (shortwave and longwave downward radiation) and freshwater fluxes (total precipitation and snow) are the daily climatology of DFS5.2 (period 1979-2010). This was also the strategy for DFS5.1, DFS4 and for CORE. The backward extension of the surface atmospheric variables required for the calculation of turbulent fluxes (t2, q2, u10 and v10) makes use of the ERA40 reanalysis. Differently to DSF5.1, we do not use the common period (1979-2001) to match the two data sets because this was introducing a noticeable discontinuity in 1979. The 3-hourly "synoptic scales" of ERA40 of the period 1958-1978 are calculated as the difference between instantaneous original ERA40 fields and the ERA40 daily mean climatology (period 1958-1978). Linear trends are calculated and removed. The daily climatology of DFS5.2 (period 1979-2012) is then added to the ERA40 synoptic scale to give the instantaneous DFS5.2 fields. A consequence is that the variables in DFS5.2 show no trends over the period 1958-1978 and the climatological mean of that period is the same as for the 1979-2012 period. The whole process is described in details in Section 5. To provide a homogeneous record, all fields are provided on a 0.7° grid, every 3h for the turbulent variables and daily for radiation and precipitation. DFS5.2 has been extended to 2013.

Table 3: Major characteristics of the DFS5.2 forcing data set.

<table>
<tr><th rowspan="2">Variable name</th><th rowspan="2">Description</th><th rowspan="2">Units</th><th colspan="2">DFS5.1 Origin, time and grid resolution</th></tr>
<tr><th>1958-1978</th><th>1979-200710</th></tr>
<tr><td>u10</td><td>Zonal wind speed at 10 m height</td><td>$m.s^{-1}$</td><td rowspan="4">ERAi* daily climatology (1979-2010) combined with ERA40** 3-hourly synoptic scales (1958-1978) 0.7° resolution</td><td rowspan="4">ERAi* 3-hourly 0.7° resolution</td></tr>
<tr><td>v10</td><td>Meridional wind speed at 10 m height</td><td>$m.s^{-1}$</td></tr>
<tr><td>t2</td><td>Air temperature at 2 m height</td><td>°C</td></tr>
<tr><td>q2</td><td>Air specific humidity at 2 m height</td><td>kg/kg</td></tr>
<tr><td>radsw</td><td>Downward shortwave radiation</td><td>$W.m^{-2}$</td><td rowspan="2">ERAi* daily climatology (1979-2010) 0.7° resolution</td><td rowspan="2">ERA-interim daily 0.7° resolution</td></tr>
<tr><td>radlw</td><td>Downward longwave radiation</td><td>$W.m^{-2}$</td></tr>
<tr><td>P</td><td>Total precipitation</td><td>mm/day</td><td rowspan="2">ERAi* daily climatology 0.7° resolution</td><td rowspan="2">ERA-interim daily 0.7° resolution</td></tr>
<tr><td>snow</td><td>Snow fall</td><td>mm/day</td></tr>
</table>

* *ERAi** = ERA-interim variables after implementation of the corrections described in Section 3. ** *ERA40 resolution is 6-hourly and 1.125°. To provide a homogeneous record, ERA40 have been interpolated at the resolution of ERAi (3-hourly and 0.7°).*

1.4 Global budgets of heat and freshwater of the various DFS

We shall have a Table with global heat and freshwater budgets for all DFS forcing.

2 Brief assessment of ERAi forcing

ERAi is a recent reanalysis provided by ECMWF (Dee et al., 2011). It covers the period 1979-2013. Many improvements have been implemented to both the atmospheric model and the data assimilation system compared to ERA-40, which was the basis for DRAKKAR Forcing Set 4.3 and 4.4. The spatial and temporal resolutions have also been increased (0.7° and 3-hourly for ERAi, 1.125° and 6-hourly for ERA-40). Despite a better representation of the atmospheric state, the reanalysis still has some flaws which may significantly impact the solution of an ocean model. In order to guide the search for corrections to be applied to ERAi, we carried-out a global ocean hindcasts simulation with the global 1/4° global ORCA025.L75 configuration. This simulation is referred to ORCA025.L75.MJM95.

2.1.1 Gyre intensity

Figure 1 shows the transport across the Florida-Bahamas section, which is a good proxy for North-Atlantic subtropical gyre intensity. This section is monitored and observations (in blue) are available since 1982. We compare a DFS4.3 forced ORCA025 simulation (in black) and an ERA-interim forced ORCA025.L75 simulation (in red). The transport collapses in the ERA-interim forced simulation, which is the result of a weakening of the subtropical gyre circulation. This behaviour is observed in a large number of ERA-interim forced simulations performed by the DRAKKAR group and is not due to vertical resolution, nor to spin-up. Hence we can conclude that gyre circulation has to be strengthened, which can be achieved by increasing the wind module. The weak winds in ERAi has also been pointed out in the study of Meinvielle et al. (2013) which suggests an underestimation of the wind speed by 0.5 m/s in the inter-tropical band.

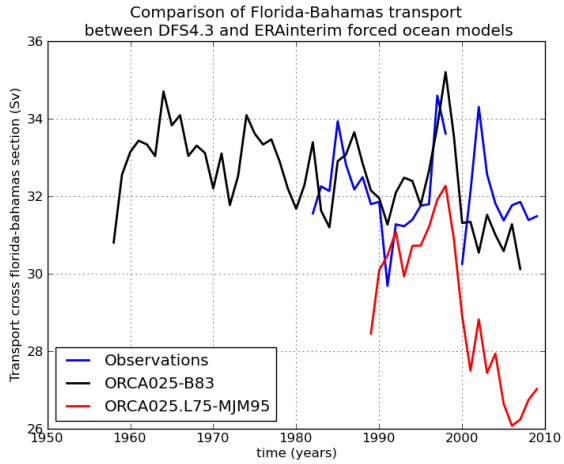

*Figure 1. The Florida-Bahamas transport in two different ORCA025 hincast simulations is shown. One is driven by DFS4.3 forcing (**black**) and the other is driven by ERAi raw forcing (**red**). The Cable observations are in **blue**.*

2.1.2 Freshwater input

Figure 2 shows the sea surface salinity restoring term in an ERAi forced ORCA025.L75 simulation. We can identify several areas where the restoring term is important: the western equatorial Pacific and Indian oceans, the equatorial Atlantic and along US/Canada East coast. The precipitations are intense and likely overestimated at low latitudes and underestimated at mid-latitudes. Similar results were found comparing ERAi to other precipitation estimates satellite or other reanalyses (Sommer, 2013). ERAi provides daily precipitations at 0.7° resolution, which brings more variability to the system than the monthly satellite-based precipitations of DFS4.3. However, to be useful, the precipitations need to be in good agreement with observations. Hence a major issue is to decrease precipitations at low-latitude

which will affect the global hydrological cycle, which is already not balanced in ERAi, showing an excess of evaporation (E-P-R = 0.33 mm/day). Despite of this non-balanced freshwater budget, simulations forced by ERAi without sea surface salinity restoring show an important negative salinity drift (freshening), leading to a sea surface rise of 50-60 cm in 20 years in both ORCA2 and ORCA025 simulations.

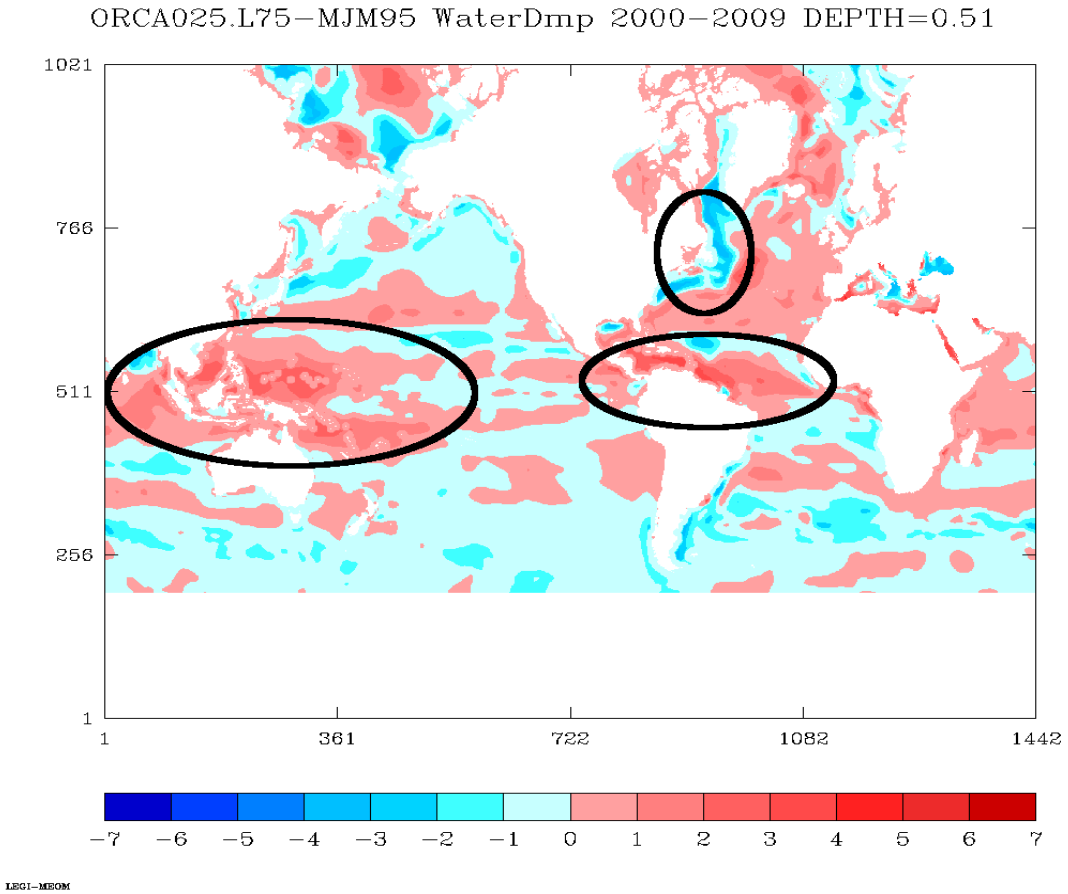

Figure 2: Mean Sea Surface Salinity restoring term in an ERAi forced simulation (2000-2009 mean). Positive (red) values means that the restoring acts similarly as evaporation, negative (blue) values means that the restoring brings freshwater.

2.1.3 Radiation fluxes

ERAi also provides daily radiation fluxes at 0.7° resolution, whereas satellite-based DFS4.3 radiation fluxes have only a 2.5° resolution. Figures 3&4 show the difference in downward shortwave and longwave radiation between ERAi and DFS4.3 (the latter being basically the satellite ISCCP product). ERAi shortwave radiations are likely overestimated (the difference with DFS4.3 being positive almost everywhere), in particular in the eastern part of ocean basins. In these latter regions the difference in longwave radiation is negative (ERAi providing less downward longwave radiation), which suggests that the discrepancies in the radiation fluxes between ERAi and satellite products are due to flaws in cloud cover representation.

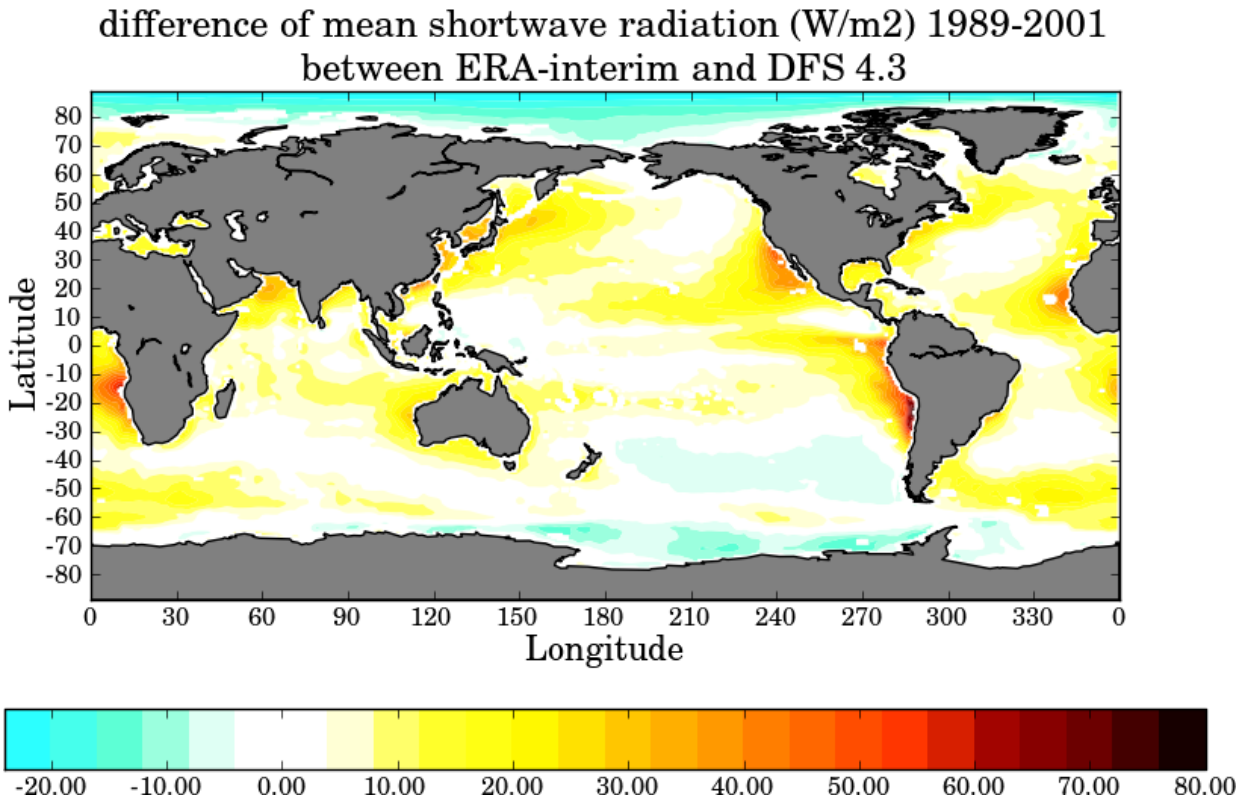

Figure 3. Difference between ERAi and DFS4.3 downward shortwave radiation (mean 1989-2001)

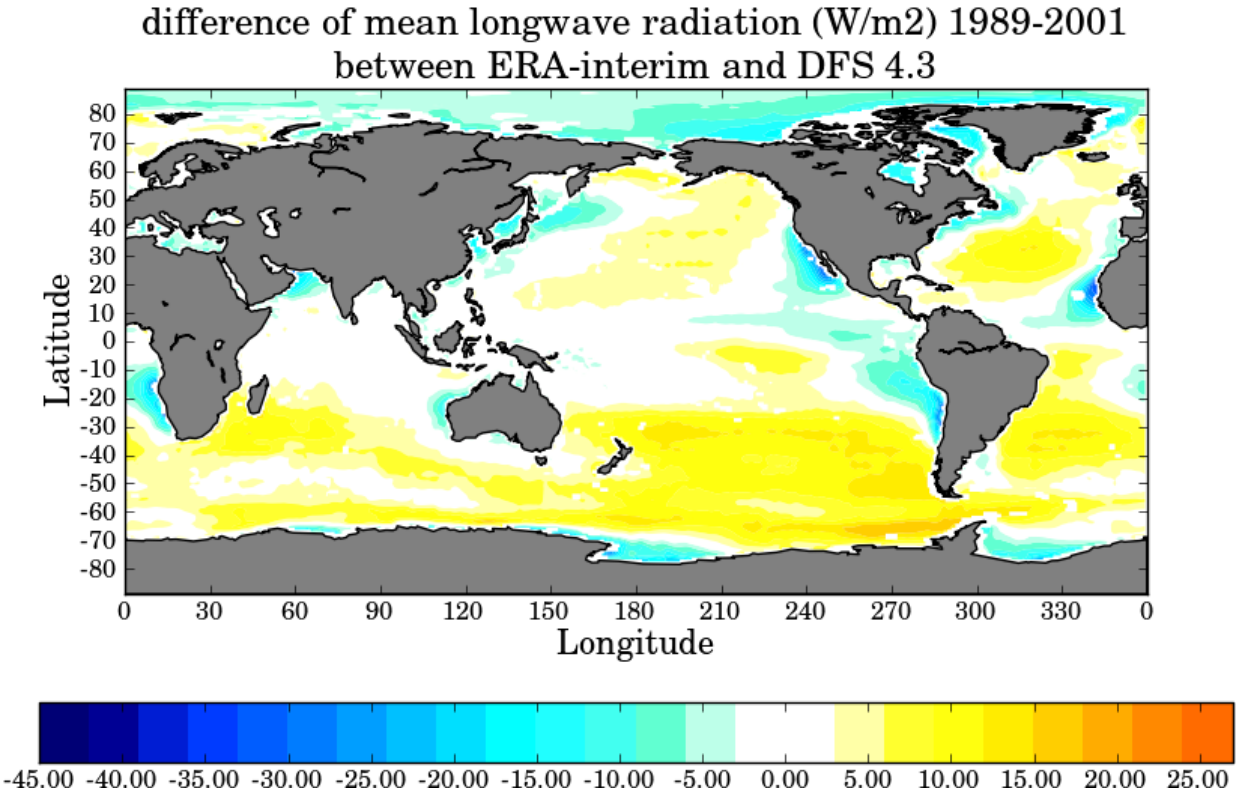

Figure 4. Difference between ERAi and DFS4.3 downward longwave radiation (mean 1989-2001).

3 Correction to ERAi for the period 1979-2010

This section describes the modifications applied to the ERAi surface variables that yielded the DFS5.1 and DFS5.2 forcing sets for the period 1979-2010 (later extended to 2012). The extension backward in time until 1958 of DFS5.2 to span the whole period 1958-2012 yielded the final DFS5.2 forcing data set.

In this section, we describe corrections common to DFS5.1 and DFS5.2 and those specific to DFS5.2. We explain how we have corrected t2 & q2 in the Arctic and in the Southern ocean. The resulting improvements in the representation of the sea-ice obtained in a coarse resolution model are then assessed. This modification is very local and does not affect much the global balances. Then, we discuss more precisely the method used to increase the wind strength, which has significant consequences on the heat and freshwater budgets (-3.77 $W.m^{-2}$ and -3.83 mm/day). Corrections of radiation fluxes are then described. The effects of those corrections on the global heat balance are -3.8 $W.m^{-2}$, which is important if compared to the net heat flux associated to global warming (which estimates vary around +0.5 W/m^2) but is still within the error bar of air-sea fluxes estimates. Corrections applied to precipitation are described. This has been a difficult task since the constraint of preserving a closed freshwater budget had to be satisfied while applying those spatial corrections. The results of coarse-resolution model (ORCA2) sensitivity simulations are sometimes used to provide assessments of the effects of the corrections.

3.1 Air temperature and humidity in the Arctic and Southern Oceans

3.1.1 Arctic: corrections common to DFS5.1 and DFS5.2

Given that the ECMWF reanalysis ERAi is much warmer/moister than DFS4.3 in the Arctic (Fig. 5), we apply similar corrections on air temperature and humidity at 2 meters than those proposed by Brodeau et al. (2010). Those corrections are based on the POLES monthly climatology for air temperature (http://iabp.apl.washington.edu/data_satemp.html). They are applied only over sea-ice-covered regions, using a monthly climatology of ice-fraction based on SSM/I satellite data. The POLES air temperature and SSM/I ice-cover climatologies (period 1979-1998) have been used. The method then consists in computing a climatological monthly offset of air temperature between the atmospheric reanalysis and POLES observations. Then a correction based on this offset is applied to the high-frequency fields. Corrections reduce the mean air temperature by more than 0.6°C everywhere in the Arctic except in the Baffin Bay where it is slightly less. The strongest correction is applied above the Laptev Sea, the Lincoln Sea and close to the North Pole along the Beaufort gyre. Regions where the mean correction is particularly important are also found over the Barents Sea and the Greenland Sea but on smaller length scales. The effect of the corrections on the ERAi air temperature and humidity are discussed in Section 4.

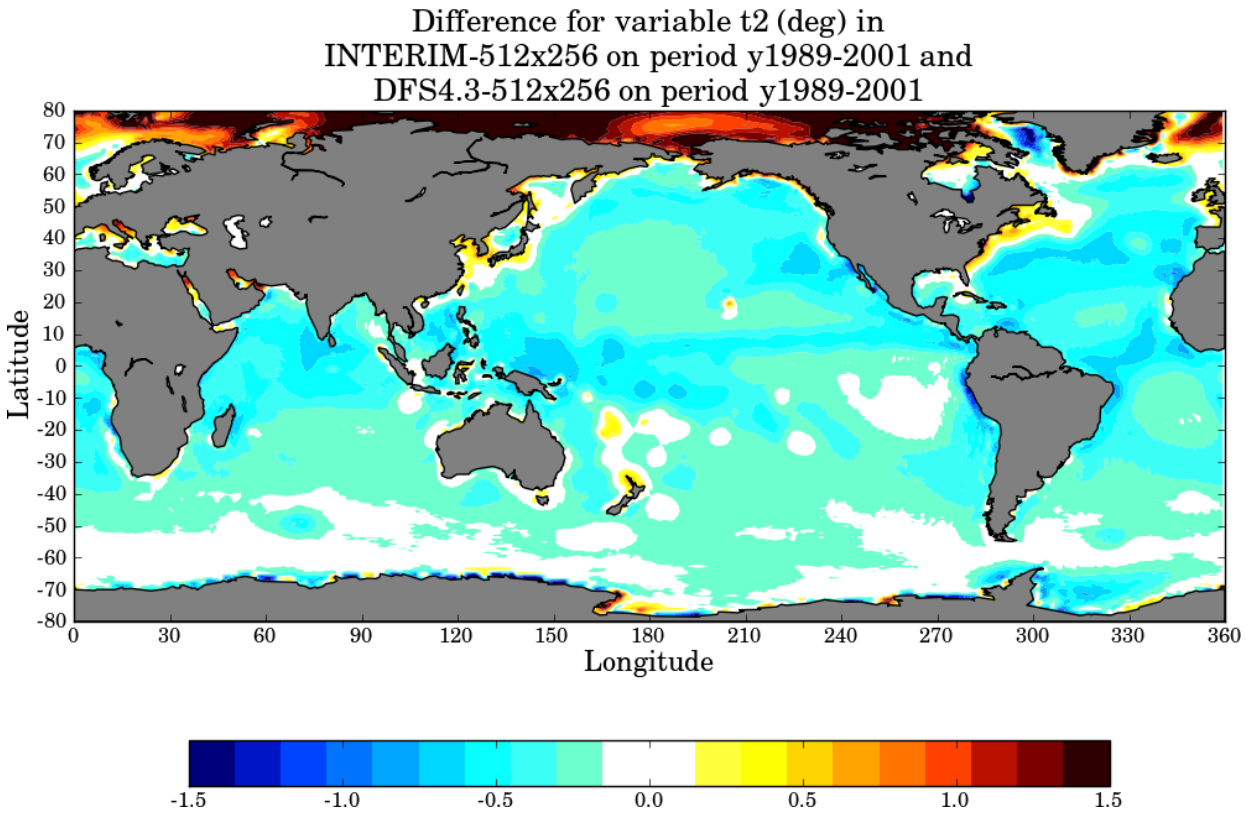

Figure 5. Difference in air temperature between ERAi and DFS4.3 (1989-2001 mean). Units are °C.

Figures 6&7 show the sea-ice area and extent in respectively March and September in two ORCA246 (2° and 46 vertical levels) simulations compared to observations from NSIDC (blue curves). The reference ORCA246 simulation (forced by the original ERAi) is shown with red curves and the corrected ERAi (with only air temperature and humidity corrections in the arctic) is shown with black curves. It appears that the reduction of air temperature gives an overestimation of ice area in winter but a better extent. In summer, there is a major improvement of both ice area and extent. As this modification was already applied to ERA-40 in order to build DFS4.3, it was relevant to reproduce it on ERAi to build DFS5. These modifications give good results on sea-ice properties and have a very minor impact of global net heat flux.

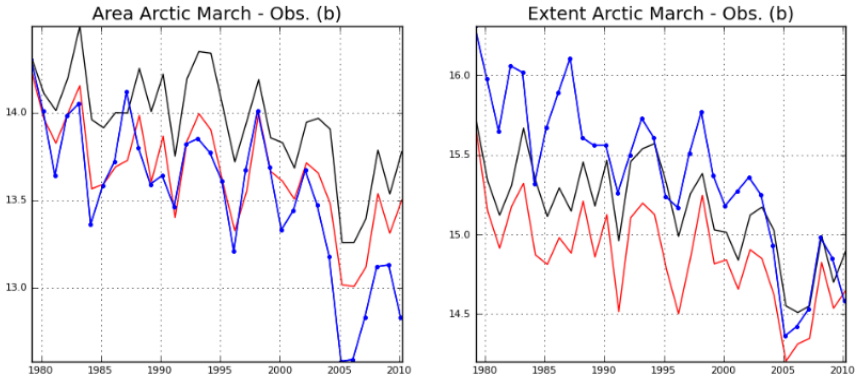

Figure 6. Ice area and extent in March in two ORCA246 simulations forced by the original ERAi (red) and the corrected-ERAi (black). Blue curves are observations from NSIDC. Units are in 10^6 km^2.

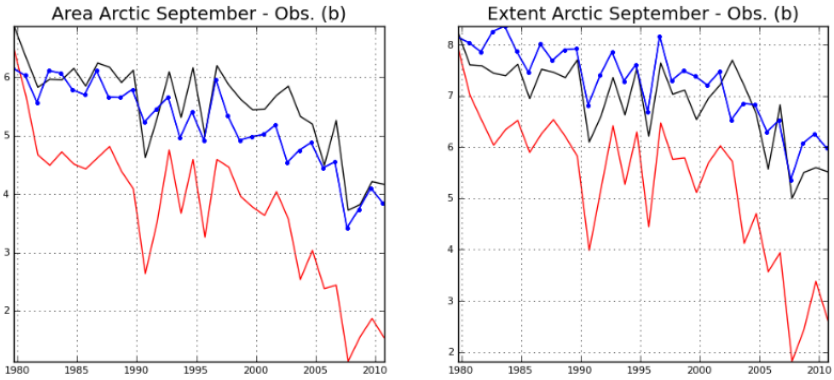

Figure 7. Ice area and extent in September in two ORCA246 simulations forced by the original ERAi (red) and the corrected-ERAi (black). Blue curves are observations from NSIDC. Units are in 10^6 km^2.

3.1.2 Southern Ocean: corrections specific to DFS5.2

ERAi air temperature is found to present an important warm bias over the whole Antarctic continent (more than a few °C, Fréville et al., 2014). The comparison of ERAi and ERA40 near surface temperatures (after application of an orographic correction) with those measured at the coastal weather stations around Antarctica (Bracegirdle and Marshall, 2012) suggests a more contrasted picture. Most stations exhibit only a small bias (<2°C) or no significant bias, and very few a small negative bias. The picture is almost identical for ERA40 and ERAi. Mathiot et al (2012) found that ERA40 2m air temperature was ~2°C warmer in average along the coast of the Antarctic continent than that produced by donwscaling performed with a regional atmospheric model that compared well to weather station observations. They suggest that ERA40 should be corrected from that bias.

Based on these studies, we have decided to apply a cooling (and associated drying) correction of the ERAi 2m air temperature (and specific humidity). The cooling of 0.2°C per degree of latitude is applied between 60°S and 75°S and yields a 2°C cooling at 75°S.

3.2 Wind speed

ERAi forced simulations have shown to have weak gyre circulation. Other independent studies (e.g. Meinvielle et al., 2013) suggest that ERAi winds are underestimated in the inter-tropical band (30°S-30°N). This is also suggested by Figure 8 which compares the zonal mean of wind module (time-averaged over the period 2000-2006) in ERAi, DFS4.3 and QuikSCAT. ERAi have weaker values than QuikSCAT almost everywhere. The greatest discrepancies are found between 40°S and 40°N, and can be as large as 0.8 m/s at the equator. In DFS4.3, ERA-40 winds have been rescaled towards QuikSCAT so values are obviously closer but still a little bit less intense than QuikSCAT.

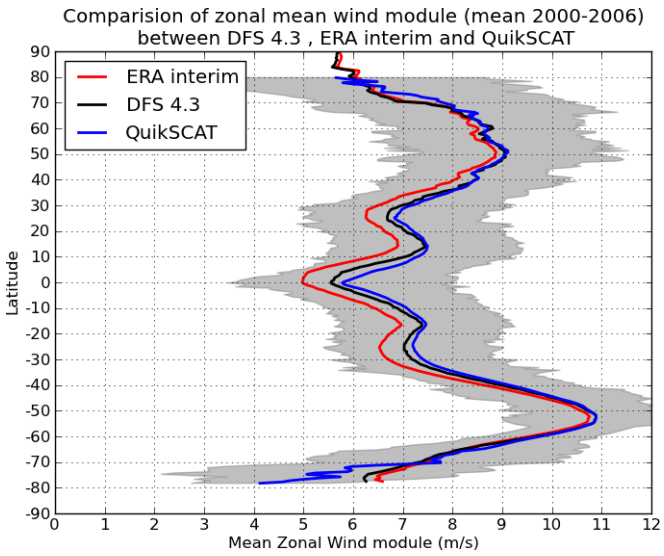

*Figure 8. Zonal average of the mean (2000-2006) 10 m wind speed. In **red** the original ERAi wind speed. In **blue** QuickSCAT wind speed estimate and its spread is shown by the grey shading. In **black** the wind from DFS4.3, i.e. the ERA40 corrected with QuickSCAT winds.*

Therefore, we decided to strengthen ERAi winds by adding a constant in time background value to the mean wind, the amplitude of which is estimated from the QuikSCAT/ERAi mean wind module ratio. As explained below, this solution has been chosen instead of straightforward multiplication by such ratio of the wind components because it yields a lower increase of evaporation.

Let us define α as the local (i.e. defined at every grid point) ratio of QuikSCAT over ERAi wind module in the formula below:

$$\alpha = \frac{\frac{1}{T}\sum_i U^i_{QuikSCAT}}{\frac{1}{T}\sum_i U^i_{ERAi}}$$

where *T* is the 2000-2008 period, *i* is the time-step and *U* is the wind module defined as:

$$U = \sqrt{u_{10}^2 + v_{10}^2}$$

The α ratio obtained by a straight calculation is somewhat noisy. A smooth ratio α_{sm} is calculated by filtering α with an anisotropic box filter. The box size is 14 grid points along the meridional direction and 28 grid points along the zonal direction, which corresponds to a 10° by 20° box. The maximum correction allowed is 15% and there is no correction above of 60°N and below of 60°S (a linear transition is done over 10 grid points, ~7° in latitude°). In practice, α_{sm} varies between 1 and 1.15 and shows small gradient to aviod any significant distortion of the divergence or the curl pattern (Figure 9). Wind speed increase is maximal at low latitudes and is also important in the Gulf Stream and the Kuroshio area. The correction brings a 0.5 to 1 Sv increase of the Florida-Bahamas transport in ORCA2 simulations, while being still very weak compared to observations due to the model viscosity. The eddy-permitting models are expected to show the similar behaviour but with changes of greater amplitude. No correction is applied beyond 60° latitude in both hemisphere, and only weak corrections are done south of 50°S. The methodology used does not have any impact on trends.

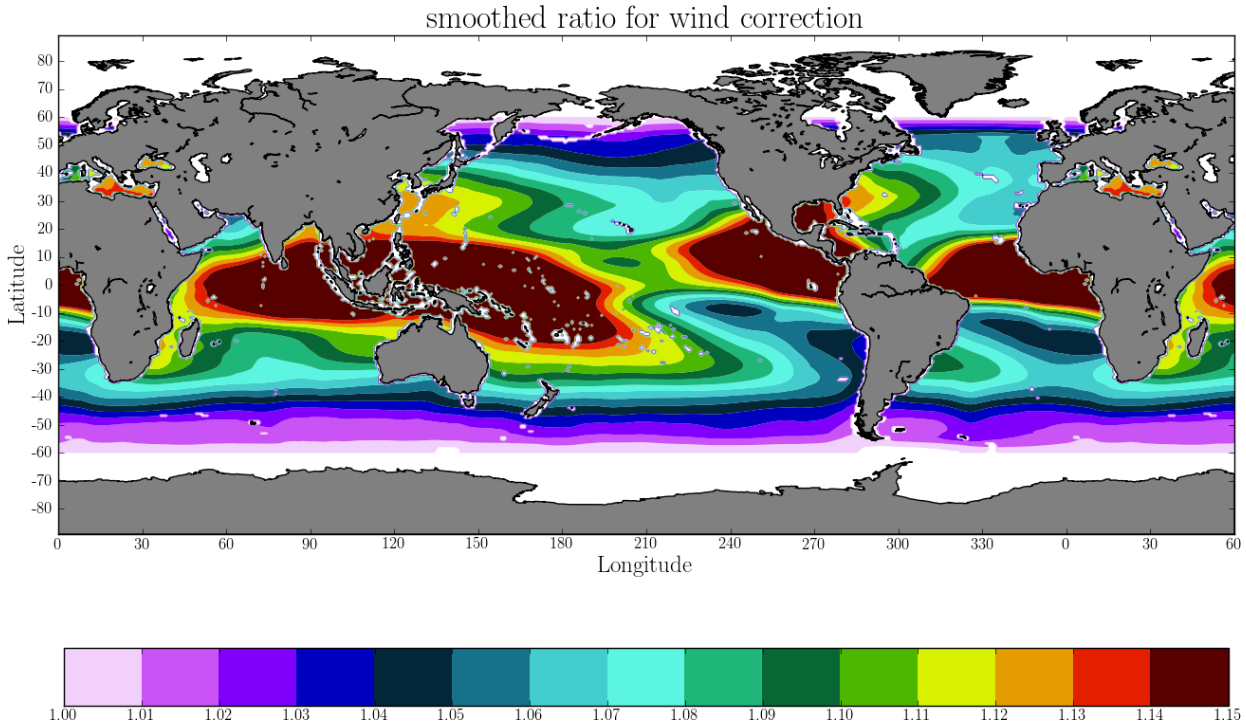

Figure 9. Multiplicative smoothed ratio α_{sm} used for wind speed enhancement.

Two different methods have been tested for the wind correction. The "multiplicative ratio" method in which the "corrected" wind speed (noted u^*_{10} hereafter) would be obtained by scaling the 10 m wind with the smooth ratio at every time-step:

$$u^*_{10} = \alpha_{sm} \times u_{10}$$
$$v^*_{10} = \alpha_{sm} \times v_{10}$$

The "background value" method (v2 hereafter) in which the smooth ratio is used to shift the mean without changing the variance of the field in the following way:

$$u^*_{10} = (\alpha_{sm} - 1) * \bar{u}_{10} + u_{10}$$
$$v^*_{10} = (\alpha_{sm} - 1) * \bar{v}_{10} + v_{10}$$

As an increase in wind speed leads to enhanced evaporation, the multiplication by a ratio gives wind increments proportional to the wind speed even in case of extreme events. This leads to much greater evaporation rates, which is something that we want to prevent since the ERAi freshwater budget is already unbalanced in favour of evaporation (by 3.3 mm/day). Note that the NCAR bulk formula used here might also be to blame for this excess of evaporation, since they significantly promote evaporation (compared to COARE for example, Brodeau & Barnier 2014, in preparation).

Figure 10 shows the difference of evaporation between the "multiplicative ratio" method (*v1*) and the "background value" method (*v2*). We clearly see that the *v2* method produces an evaporation increase of much smaller amplitude (up to 1 mm/day in the Gulf Stream). It gives an evaporation increase of 0.15 mm/day compared to the original ERAi, which is more acceptable than the 0.35 mm/day provided by the *v1* method (see Table 4), especially since this evaporation increase will have to be balanced by precipitations, already suspected as being overestimated in ERAi. Regarding the net heat flux, *v1* provides a dramatic cooling of the

ocean whereas *v2* is much closer to balance. Since radiation fluxes will also be slightly reduced, the net heat flux in *v1* is certainly too low.

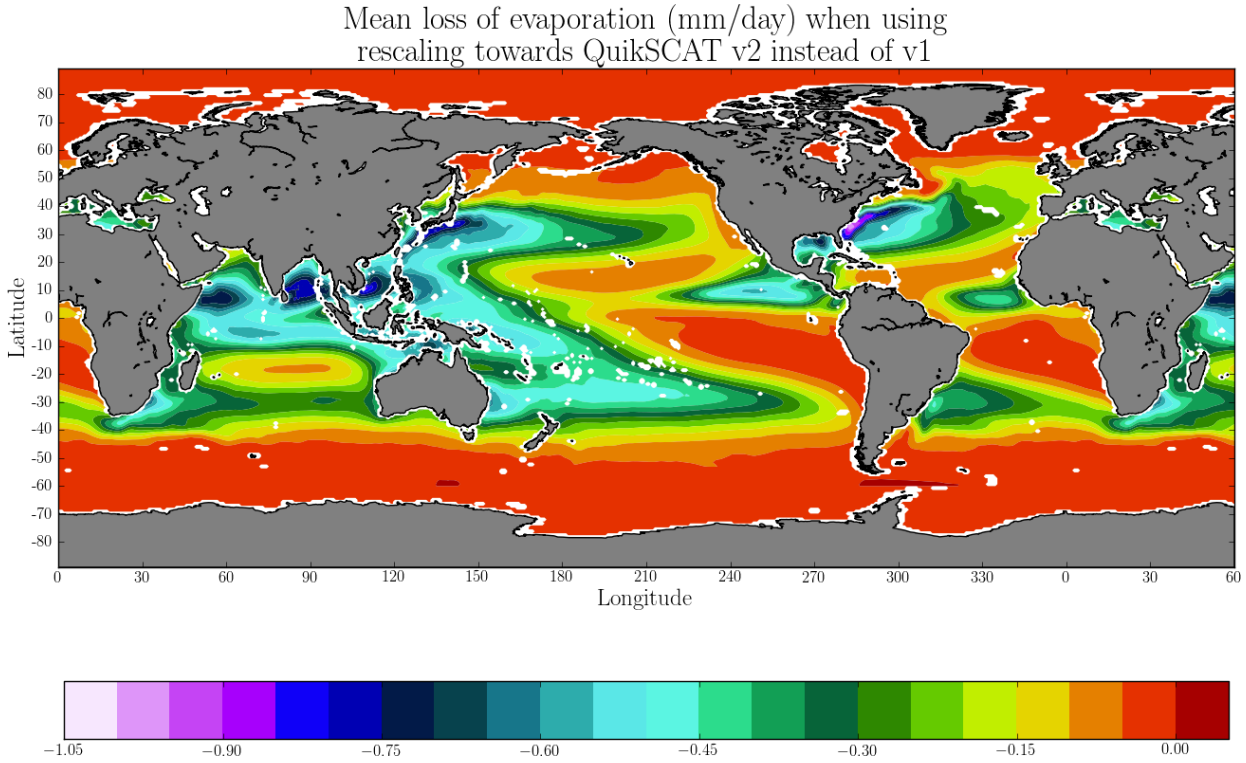

Figure 10. Differences in evaporation between the "background value" method (v2) and the "multiplicative ratio" method (v1). Negative values correspond to a diminution of evaporation in the background value method compared to multiplicative ratio method.

The effects of the corrections on the ERAi 10 m wind field are discussed in Section 4.

Table 4: Global mean evaporation and net heat flux (1979-2010 mean)

	Evaporation (mm/day)	Net Heat Flux ($W.m^{-2}$)
ERAi original	3.7	5.34
ERAi corrected by *v1*	4.05	-5.65
ERAi corrected by *v2*	3.85	0.83

Specific to DFS5.1 but not retained in DFS5.2.

To limit evaporation and cooling induced by the wind correction in DFS5.1, it has been decided to apply only 80% of the correction so that the 10 m wind components of DFS5.1 (u^*_{10},v^*_{10}) are given by:

$$u^*_{10} = 0.8 \times (\alpha_{sm} - 1) \times \bar{u}_{10} + u_{10}$$
$$v^*_{10} = 0.8 \times (\alpha_{sm} - 1) \times \bar{v}_{10} + v_{10}$$

where (u_{10},v_{10}) are the components of the original ERAi, and α_{sm} is the smooth ratio shown in Fig. 9. The full correction (100%) is applied in DFS5.2.

3.3 Radiation fluxes

Achieving a good cloud cover representation in atmospheric model is a very tough task as it requires correctly resolved dynamics, as well as humidity and aerosols concentration in the air parcel. This cloud cover will then impact radiative transfer model which ultimately provide the downward shortwave and longwave radiation driving to the ocean model. Compared to satellite products (such as Gewex - Pinker and Laszlo, 1992 - or ISCCP), it appears that ERAinterim overestimates shortwave radiation and underestimates longwave radiation, the opposite behaviour of the two radiation fluxes being consistent with the existence of a flaw in cloud representation in ERAi that consists in a lack a cloud cover, thus leading to the observed biases in the radiation fluxes. Therefore it has been decided to reduce the shortwave radiation and increase slightly longwave radiation, using DFS4.3 (which is a corrected version of the ISCCP satellite data) as our reference.

Due to seasonality of the solar radiation at the poles, the only available method is obviously the multiplicative ratio method. We choose to correct the shortwave only in regions where the difference between ERAi and DFS4.3, averaged on the period 1984-2006, is greater than 10 $W.m^{-2}$. Longwave radiation is also corrected in regions where the difference between ERAi and DFS4.3, averaged on the period 1984-2006, is less than -2.5 $W.m^{-2}$.

The local ratios of ERAi radiation over DFS4.3 radiation have calculated for both shortwave and longwave radiation. Ratios are spatially smoothed using a Gaussian filter after application of "drowning" process (i.e. extrapolation of ocean values into land) to avoid the contamination of ocean values by land value during the smoothing. A masking is applied to remove correction at high latitudes and in closed seas (Hudson Bay, Mediterranean and Red seas, Persian Gulf,...). Finally, corrected fields are obtained by simple multiplication of every daily ERAi radiation field by those ratios, which are shown in figures 11&132.

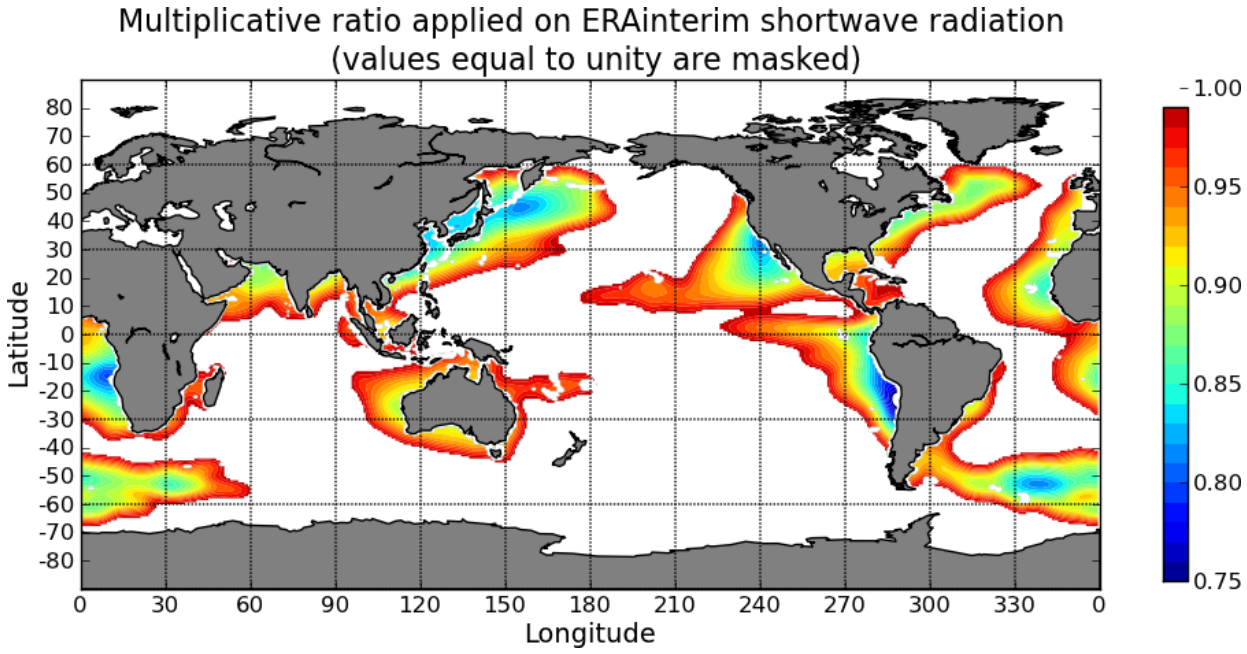

Figure 11. Multiplicative ratio applied to ERAi shortwave radiation

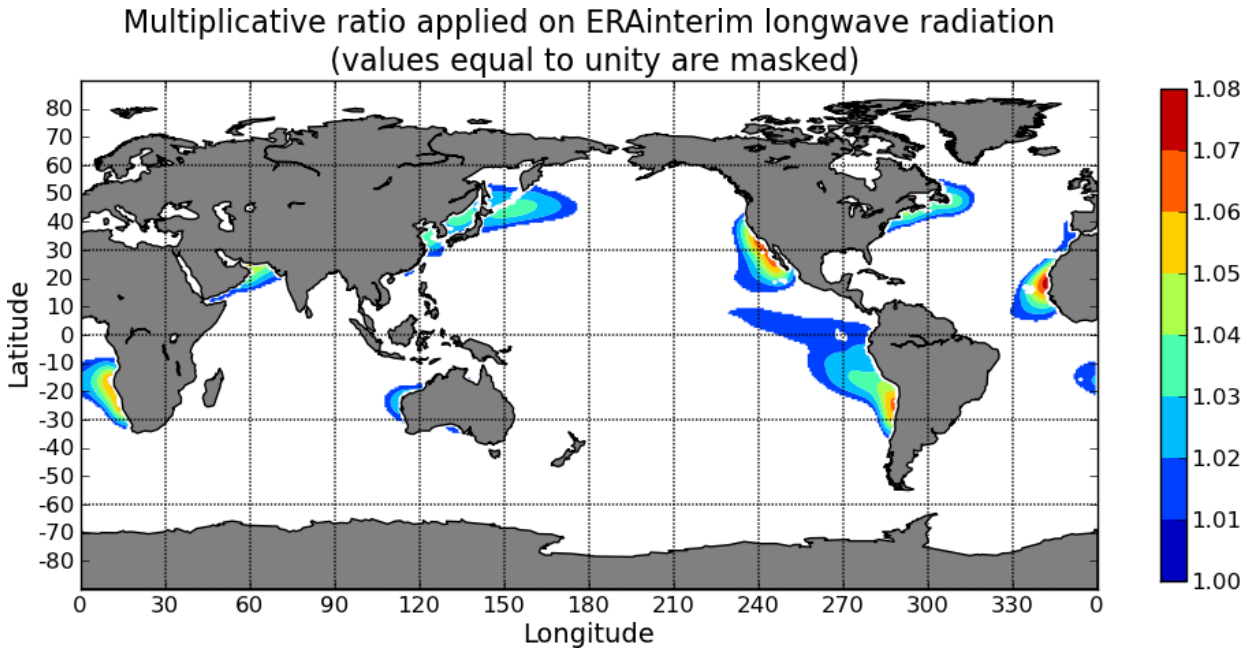

Figure 12. Multiplicative ratio applied to ERAi longwave radiation.

The effect of the corrections on the ERAi radiation fields are discussed in Section 4.

3.4 Precipitations

Regarding precipitations, various modifications have been performed. Linear trends have been removed and the corrections proposed by Storto et al. (2012) have been applied on the de-trended fields. The detrending process was motivated by the inaccuracy of precipitation trend in ERAi compared to the GPCP satellite product. Figure 13, adapted from Dee et al. (2011), shows that the precipitation trends in ERAi are not comparable to observations and these authors suggest it might be due to the variational bias correction.

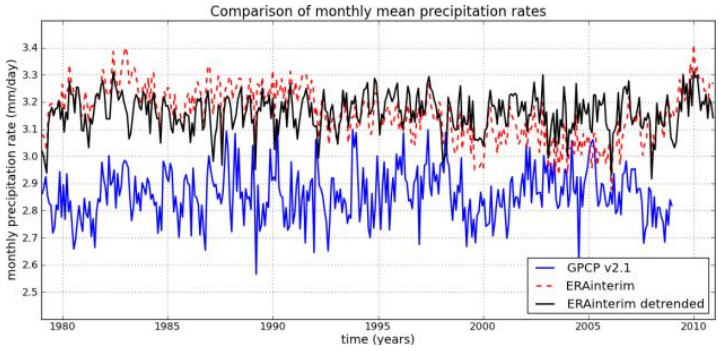

Figure 13. Monthly averaged precipitation estimates for 1979-2010 from ERAi (red), ERAi detrended (black), and GPCP (blue), averaged for all ocean locations. Adapted from Dee et al. (2011).

Figure 14 shows the globally averaged annual precipitation in ERAi as a function of time. It exhibits large variations which act to modify strongly E-P through time (Figure 15). Three periods (or time intervals) of distinct behaviour can be identified.

- A period from 1979 to 1991 when precipitations are above the mean and exhibit no trend (Fig. 14). During that period, the globally averaged annual mean E-P in ERAi is close to 0.4 mm/day (Fig. 15).
- A period from 1992 to 2004 characterized by a large "jump" (or discontinuity) in 1992 when precipitation falls by 0.13 mm/day followed by a well marked negative trend (Fig. 14). The 1992 "jump" is also noticed in the E-P field (Fig. 15), and the negative trend in P contributes to the gradual rise of E-P up to values near 0.8 mm/day.
- A period from 2005 to 2012 characterized by a strong positive trend inducing the greatest change in precipitation seen in the whole time series (0.25 mm/day). E-P decreases by almost 0.2 mm/day during that period of time (Fig. 15).

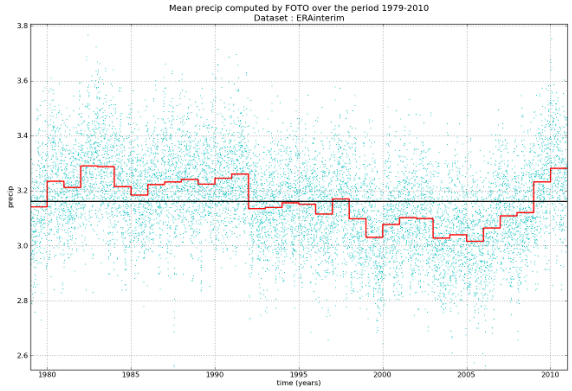

Figure 14. Globally averaged precipitation in the original ERAi (in mm/day). The blue dots are the daily values, and the red line shows the annual mean. The black line is the time mean over the whole period.

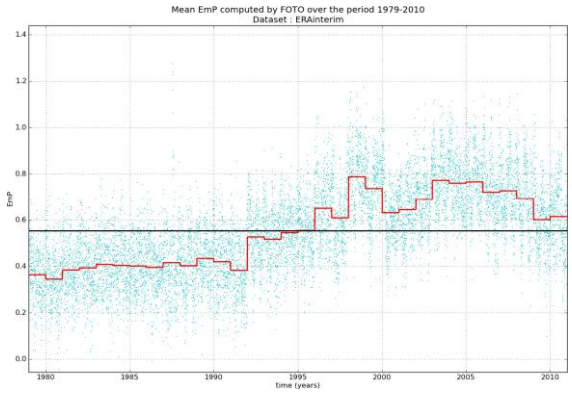

Figure 15. Globally averaged E-P in the original ERAi (in mm/day). The blue dots are the daily values, and the red line shows the annual mean. The black line is the time mean over the whole period.

Those discrepancies are likely to induce large-scale salinity drifts in ocean models. Given that uncertainties on precipitations are quite large, poor confidence should be given to those trends and discontinuities. Thus, it has been decided to correct the precipitations in order to stabilize the freshwater budget in time following an approach in two steps.

In the first step, we calculate and remove the linear trend of the precipitation time series for each of the 3 time intervals identified above independently (1979-1991; 1992-2004, 2005-2012). The process is applied at every grid point using the significant trend (two-tailed t-test) computed over the corresponding period. Figure 16 shows the result of that de-trending. Marked discontinuities (or "jumps") are clearly seen between the periods in 1992 and 2005, as the result of the piecewise de-trending approach.

In a second step, for each period, the de-trended precipitation fields have been rescaled to the original 1979-2010 mean of 3.16 mm/day to remove the "jumps" and to conserve the total

precipitation over the full ERAi period. Figure 17 shows the result of the rescaling. The impact of this correction on the E-P budget is a decrease by almost 0.2 mm/day, which goes in the right direction toward a closed E-P budget.

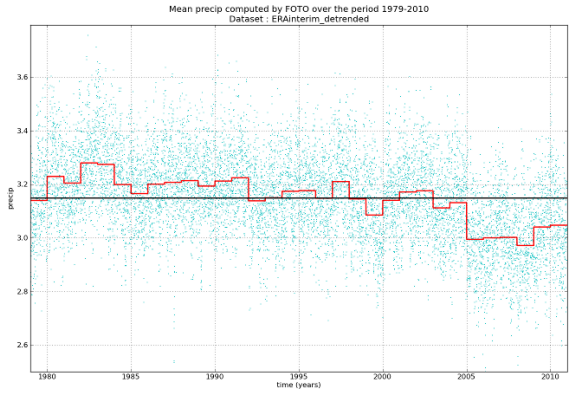

Figure 16. Globally averaged precipitation in ERAi after the application of the piecewise de-trending. The blue dots are the daily values, and the red line shows the annual mean. The black line is the time-mean over the whole period. Notice the steps in 1992 and 2005 due to de-trending by pieces and the mean value (black curve) is lower than in ERAi.

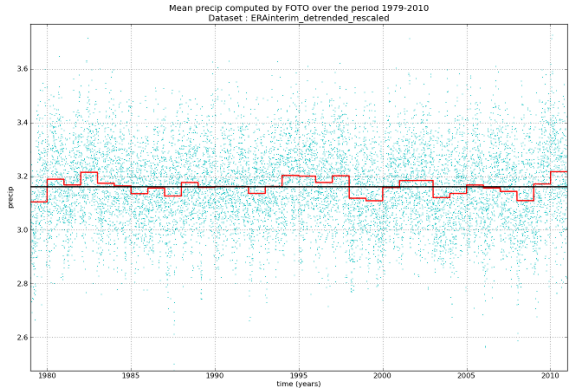

Figure 17. Globally averaged, de-trended and re-scaled precipitation in ERAi. The blue dots are the daily values, and the red line shows the annual mean. The black line is the time-mean over the whole period. There is no more discontinuity in 1992 and 2005 and the mean is back to the original value.

Finally, we have applied the method of Storto (personnal communication, 2013) to the de-trended precipitations with a few modifications. The method is designed to work online (in sbcblk_core module) in the case of an ORCA025 simulation. As our purpose is to provide a standalone corrected forcing set on the native ERAi grid, we adapted Storto's code to run it offline. However interpolation to ORCA025 was needed to apply the correction, thus fields have been interpolated twice: from native to ORCA025 grid before correction then from ORCA025 to native grid after correction.

Storto's method separates the large scales from the small scales precipitations with a dimensional low-pass Shapiro filter, tuned to have 20% amplitude attenuation at the spatial scales corresponding to 900km. A spatially varying, monthly climatological scaling coefficient is computed over the period 1989–2008 that accounts for the ratio between the ERAi large scale precipitation and a satellite-based passive microwave precipitation product (the PMWC product, Hilburn, 2009). The large scale ERAi precipitation is then scaled with this coefficient and the small scale precipitation are added back. Whereas Storto suggests to interpolating in

time the correction term, we found it inappropriate because what we consider important to conserve the total amount of added (or retrieved) precipitations over the month.

Figure 18 shows the correction provided by Storto's method on original ERAi (not de-trended). Though the obtained corrected field (after de-trending) will be slightly different (see next section), this illustrates the main effects of this correction. The correction decreases the mean precipitation in the western tropical Atlantic and Pacific oceans which will allow to reducing the freshwater biases found in ERAi-driven simulations in these regions. Precipitations are also increased in northern hemisphere subtropical gyres with a strong increase along Canadian east coast which is more surprising.

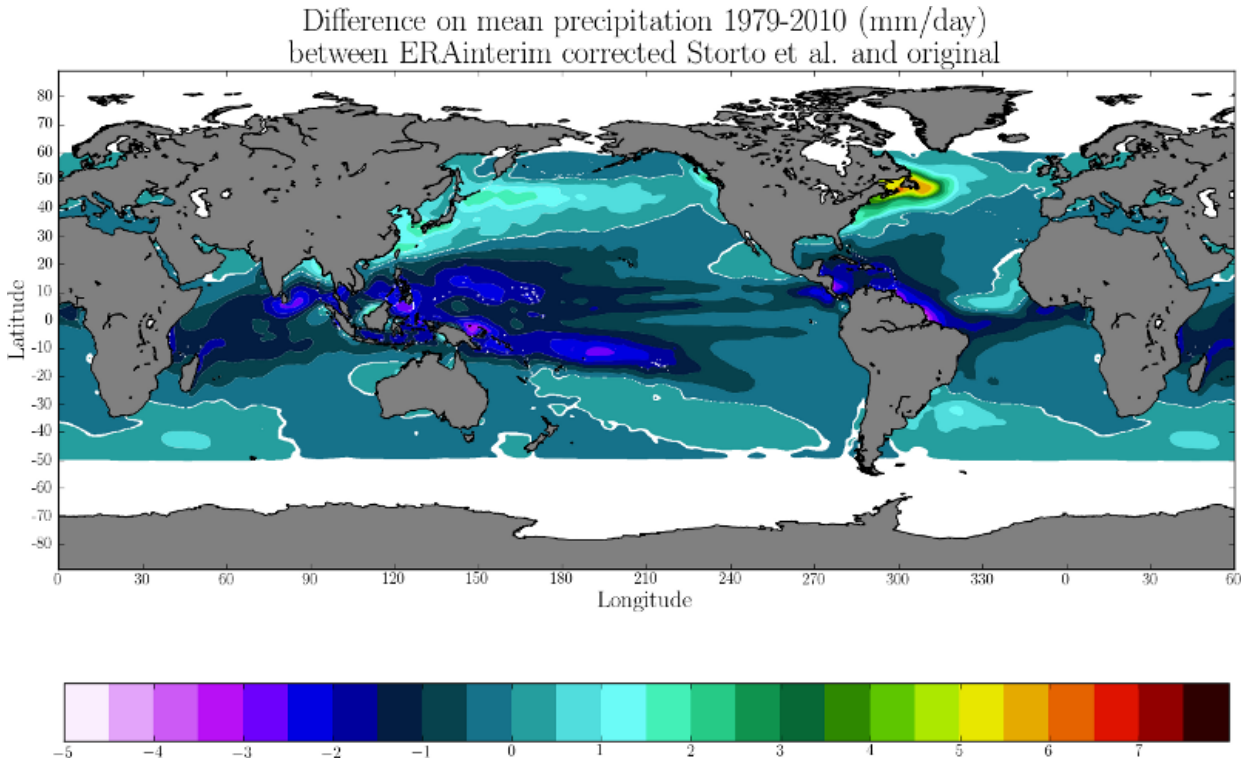

Figure 18. Mean (1979-2010) precipitation difference between the ERAi data corrected with Storto's method and original ERAi data.

In the next section, we show the results of all the modifications performed on ERAi. We focus on the differences between DFS5.2 and the original ERAi and provide information mostly on the climatological mean and interannual variations. This is presented as an atlas to give the essential information about DFS5.2. More exhaustive diagnostics are available in the FARC reports (available at http://www.drakkar-ocean.eu/forcing-the-ocean).

4 Extending DFS5.2 to the period 1958-1978

ERAi is limited to the period 1979-2012 and consequently so is DFS5.2. This section describes the final stage of the making of DFS5.2: the extension of DFS5.2 backward over the years 1958 to 1978 using ERA40 reanalysis to finally span the period 1958-2012. The extension process yields the final DFS.2 which covers the period 1958-2012. Assessment of DFS5.2 is being carried out with ocean hindcasts at 1°, 1/2°, 1/4° and 1/12° resolution. In the following, when fluxes are presented, they have been calculated using the Bulk formula of Large and Yeager (2004) and the interannually varying SST of Hurell et al. (2008).

4.1 Radiation and freshwater fluxes for 1958-1978

Regarding radiation (downward shortwave and longwave) and freshwater (total precipitation and snow) fluxes, the lack of observations before 1979 and the large flaws noticed in ERA40 reanalysis did not allow to produce reliable enough inter-annually varying fluxes. Therefore, we decided to use the daily climatology of DFS 5.1 (being calculated over the period 1979-2010). This was also the strategy for DFS4 and is also the strategy used in CORE. The extension is illustrated in Fig. 20 with the shortwave radiation in the equatorial band and the global precipitation, respectively. There is a lack of high frequency variability for the period before 1979 due to the use of the daily climatology. However, the continuity of the record through 1979 is well assured and the whole record is centred on the 1979-2012 mean value.

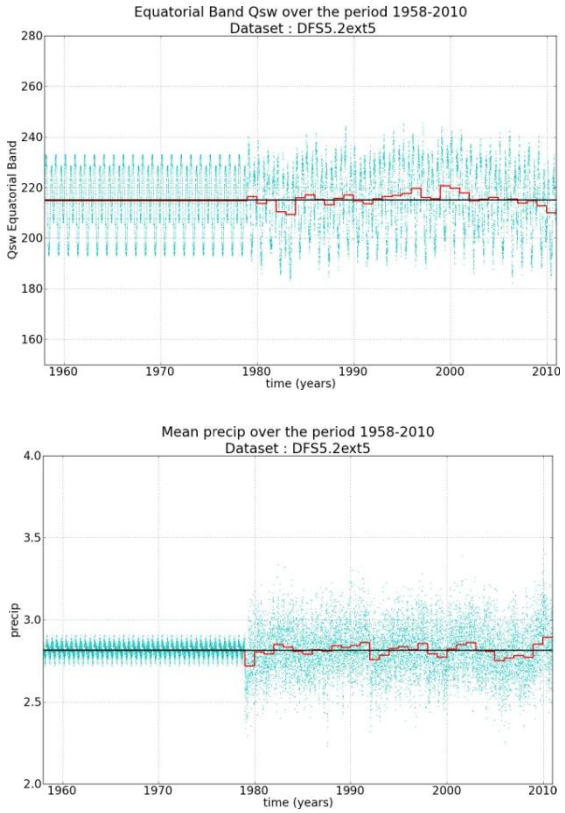

Figure 20. Time-series of (upper plot) the zonal average in the equatorial band of the shortwave radiation (W.m^{-2}) and (lower plot) the globally averaged precipitation in DFS5. Blue dots are daily values. The red line shows the annual mean. The black line is the time-mean over the whole period.

4.2 Turbulent fluxes for 1958-1978

For the atmospheric variables required for the calculation of the turbulent fluxes (t2, q2, u10 and v10), the strategy is much complex is based on an approach that combines DFS5.1 daily climatology to the high frequency of the synoptic scales of ERA40. This is done in several steps detailed below (Figure 21):

i. Compute the mean state for each variable: we produce a daily climatology for every variable of DFS5.2 for the period 1979-2012 and of ERA40 for the period 1958-1978.
ii. 6-hourly *residues* are computed for ERA40 over 1958-1978: we remove from the ERA40 full 6-hourly fields the ERA40 daily climatology computed above and remove any significant linear trend. ERA40 *residues* are interpolated to 3-hourly time frequency: to avoid changes in time frequency between the extended and standard periods, a linear interpolation is performed in time on the residues.
iii. The full fields for DFS5.2 over 1958-1978 is recomposed by adding the 3-hourly residues of ERA40 to the daily climatology of DFS5.2. All fields are given on the 0.7° original ERAi grid.

The resulting time-series are shown in Fig. 22 for the zonal wind component in different latitude bands. There is a rather good continuity between the two periods 1958-1978 and 1979-2010 and no major jumps in 1979. Though the effective time frequency over the period 1958-1978 is only 6 hours, the amplitude of the time-series is rather similar for the two periods.

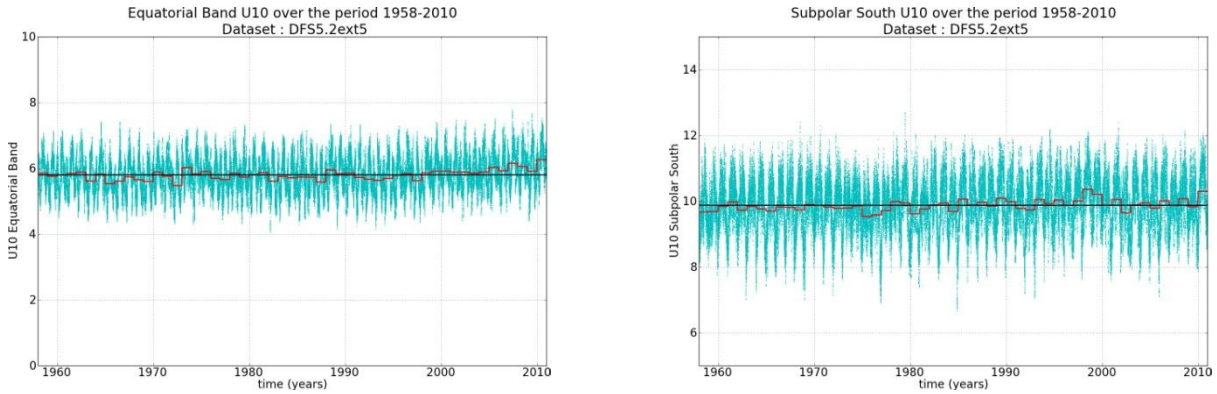

Figure 22: Zonal average of the zonal component of the 10 m wind in DFS5. Left: in the equatorial band (10°S-10°N). Right: in the Southern Ocean (45°S-70°S). The record shows a very continuity between the ERA40 and the ERAi periods. A small increasing trend is noticeable from the late 1990s to present in the equatorial band. A small increasing trend is noticeable from the mid 1970's to the late 1990's in the Southern Ocean. Blue dots are 3-hourly values. The red line shows the annual mean. The black line is the time-mean over the whole period.

Fig. 23a-c shows the global average of the net heat flux, Qnet, and of its two major components, the total radiation flux Qrad and the total turbulent flux Qtrb. There is no apparent "jump" in 1979 when the ERA40 and ERAi data sets are joined. However, there is a clear shift between the two periods in term of mean value, shift mainly driven by Qtrb (and more specifically by the latent heat flux). Qtrb does not vary much over the first 20 years of the record (nearly 115 Wm^{-2} from 1958 to 1975), but increases rapidly by nearly 10 Wm^{-2} between 1976 and 1984 (without any marked discontinuity in 1979). Qtrb shows an increasing trend for the rest of the period (from the 1980's to present), trend also seen in COREv2. The global freshwater flux (not including runoff) E-P, shown in Fig 23d, exhibits a discontinuity in 1979,

comparable to the change in P seen in 1998 or 1999. It is mainly driven by P and by the shift from daily climatology to inter-annually varying (see Fig. 20).

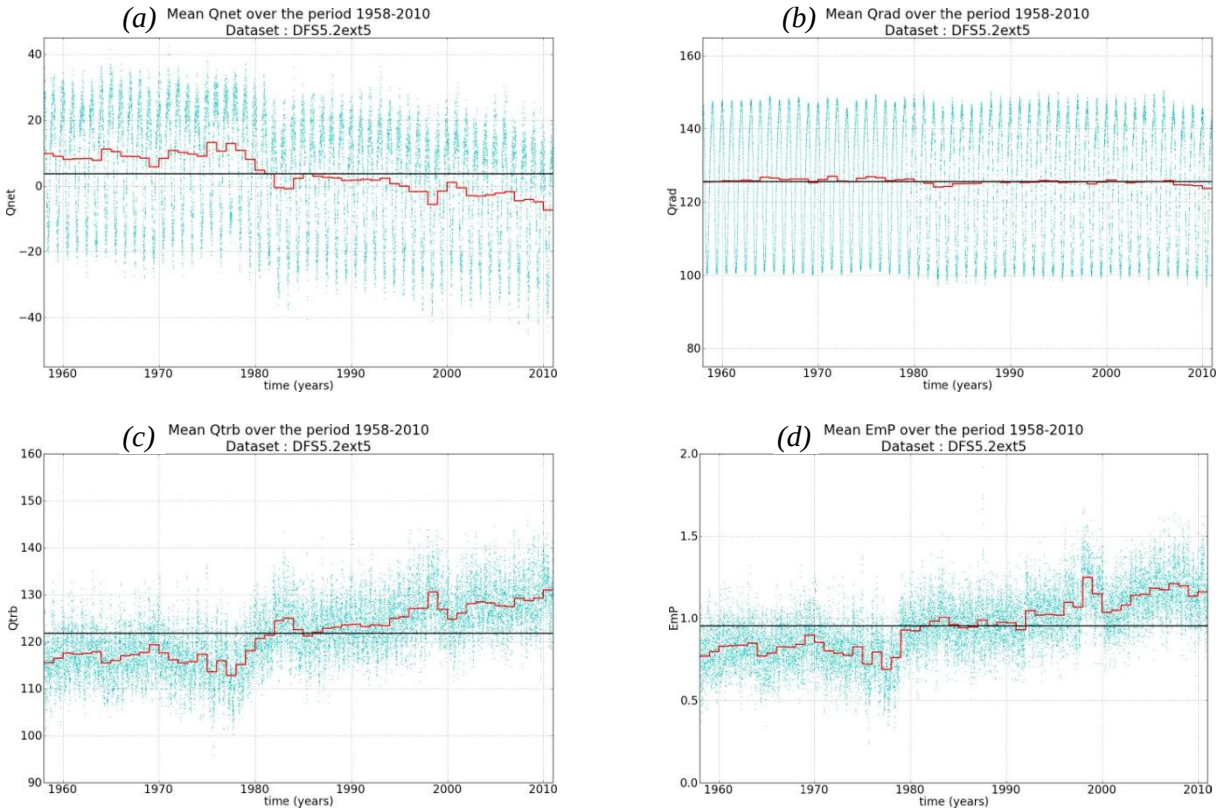

Figure 23. Global average of (a) the Net Heat Flux Qnet and its two major components, the total radiation flux Qrad (b) and the total turbulent flux Qtrb (c).Units are in Wm^{-2}. The global freshwater flux (not including runoff) E-P (mm/day) is shown in (d). Blue dots are 3-hourly values. The red line shows the annual mean. The black line is the time-mean over the whole period.

5 Atlas of comparisons between DFS5.2 and original ERAi

Work in progress.

This section will provides the reader with a complete atlas of differences between DFS5.2 and ERAi for every atmospheric variable, focusing on the climatological mean calculated over the period 1979-2012 (map of differences, zonal means and its difference) as the well the inter-annual time-series. Plots are presently being done. The reader who needs more detailed information can request the so-called FARC (Flux Atlas Revolutionary Computation) report. This report provides several maps, time-series and trends for every flux and every atmospheric variable.

6 References

Work in progress

Brodeau et al., 2012. An ERA40-based atmospheric forcing for global ocean circulation models. Ocean Modelling, Volume 31, Issues 34, 2010, Pages 88-104, ISSN 1463-5003

Storto A., I. Russo , and S. Masina, 2012. Interannual response of global ocean hindcasts to a satellite-based correction of precipitation fluxes. Personnal communication.

Dee et al., 2011. The ERA-Interim reanalysis: configuration and performance of the data assimilation system. Quart. J. R. Meteorol. Soc., Volume 137, Pages 553-597.

Pinker R.T. and I. Laszlo, 1992: Modeling Surface Solar Irradiance for Satellite Applications on a Global Scale, J. Appl. Met., 31, 194-211).

To be completed:

Large and Yeager, 2004

Zhang et al., 2004

Hurrell et al 2008.

Rigor et al., 2000

Mathiot et al., 2010

Le Sommer et al., 2013

Meinvielle et al., 2013

Hilburn, 2009